Primary Steps in the Reaction of OH Radicals with Amino Acids at Low Temperatures in Laval Nozzle Expansions: Perspectives from Experiment and Theory†

Matthias Liessmann,† Björn Hansmann,† Patrick G. Blachly,§ Joseph S. Francisco,§ and Bernd Abel*,‖

Institut für Physikalische Chemie der Universität Göttingen, Tammannstrasse 6, 37077 Göttingen, Germany, Department of Chemistry, Purdue University, West Lafayette, Indiana 47907-2084, and W.-Ostwald-Institut für Physikalische und Theoretische Chemie der Universität Leipzig, Linné-Strasse 2, D-04103 Leipzig, Germany

Received: February 20, 2009; Revised Manuscript Received: April 27, 2009

Recent work has focused on the damaging effects of free radicals on biological molecules. This study investigates the kinetics of the attack of OH radicals on L-alanine ethyl ester in the gas phase in cold beams of Laval nozzle expansions. Experiments and high-level theory are used to understand the preferred site of attack by the OH radical. Optimizations of L-alanine and L-alanine ethyl ester show that the essential transition state features for hydrogen abstraction off the C_α, C_β, and N are similar. The energetics show that for L-alanine, the C_α-site, C_β-site, and N-site transition states are all below the reactants level. For L-alanine ethyl ester, however, the energetics for hydrogen abstraction off the C_α and N are the preferred site of reaction. These findings are supported by the observed negative temperature dependence of the rate constants of OH with alanine ethyl ester in Laval nozzle expansion experiments. More importantly, both the experiments and theory show that L-alanine ethyl ester provides a good model for gas phase studies of the amino acids such as L-alanine.

1. Introduction

Amino acids are the main building blocks of living systems, being the principal components of all natural peptides and proteins. It has been established that the structure of amino acids in peptides and proteins can be severely damaged in the presence of free radicals such as OH.[1−3] It has been proposed that the oxidative damage caused by free radicals on proteins and other biological molecules may be involved in the development of cancer as well as cardiovascular and Alzheimer diseases.[4] As a first approximation, the attack of an OH radical on a protein can be considered as an attack on one of its amino acids. This reaction is the first step in a complex mechanism, which ends with the fragmentation of the peptide chain of the protein. The full mechanism of such a reaction is still unknown. It has been reported that α-carbon-centered radicals may play a decisive role in the reaction chain.[5] A number of studies in the condensed phase have been reported.[6−11] The reaction of OH with amino acids has been investigated in aqueous medium experimentally and there are theoretical studies in the gas phase.[12−18] Up to the present no experiments in the gas phase have been published. The sites of reaction in general appear to be the subject of discussion: Radiolysis in the condensed phase followed by ^{1}H/^{2}H exchange lead to the conclusion that side chains are the primary reactive site,[19] whereas other studies prefer N-centered radicals or the α-carbon as the site of attack.[5] In theoretical studies by Galano et al.[17] on isolated L-alanine and glycine it was found that α-carbon and β-methyl hydrogen abstraction reactions are favored, with the α-carbon attack in L-alanine proceeding via the lowest barrier. By use of experiment and theory the present work aims to examine the attack of OH with L-alanine and L-alanine ester to understand the mechanistic details of the abstraction process in the gas phase at low temperatures.

2. Experimental Section

The pulsed Laval nozzle machine used in Göttingen has been described in detail elsewhere,[20−22] therefore only a short description is given, focusing on the experimental features specific for the experiments presented here. Figure 1 displays a typical experimental scheme. A pulsed Laval nozzle is used to generate a low-temperature environment for the molecular processes under investigation.

The wall curvature of the nozzles has to be designed for a specific flow gas, temperature, and density in the gas jet. The Mach number M and the adiabatic coefficient denoted γ characterize the flow conditions. The relations between M and thermodynamic properties are given in eqs 1−4. The pressure in the stagnation region, p_0, the impact pressure of the flow, p_i, and the background pressure in the reaction chamber, p_{bg}, are usually measured to control the flow conditions. The temporal evolution of the stagnation pressure is displayed in Figure 1. A throttle valve conveniently adjusts the background pressure in the chamber. The characterization of the flow conditions is achieved by measuring the impact pressure p_i and the pressure in the stagnation volume p_0 to calculate the Mach number ($\gamma = c_p/c_v$)

$$\frac{p_i}{p_0} = \left[\frac{(\gamma+1)M^2}{(\gamma-1)M^2+2}\right]^{\gamma/(\gamma-1)}\left[\frac{\gamma+1}{2\gamma M^2-\gamma+1}\right]^{1/(\gamma-1)} \quad (1)$$

The flow conditions are now determined using the Mach number calculated from the impact pressure data. The relation

† Part of the "Robert Benny Gerber Festschrift".

* Corresponding author, bernd.abel@uni-leipzig.de, fax +49-(0)341-9736399.

† Institut für Physikalische Chemie der Universität Göttingen.

§ Department of Chemistry, Purdue University.

‖ W.-Ostwald-Institut für Physikalische und Theoretische Chemie der Universität Leipzig.

10.1021/jp9015596 CCC: $40.75
Published on Web 05/21/2009

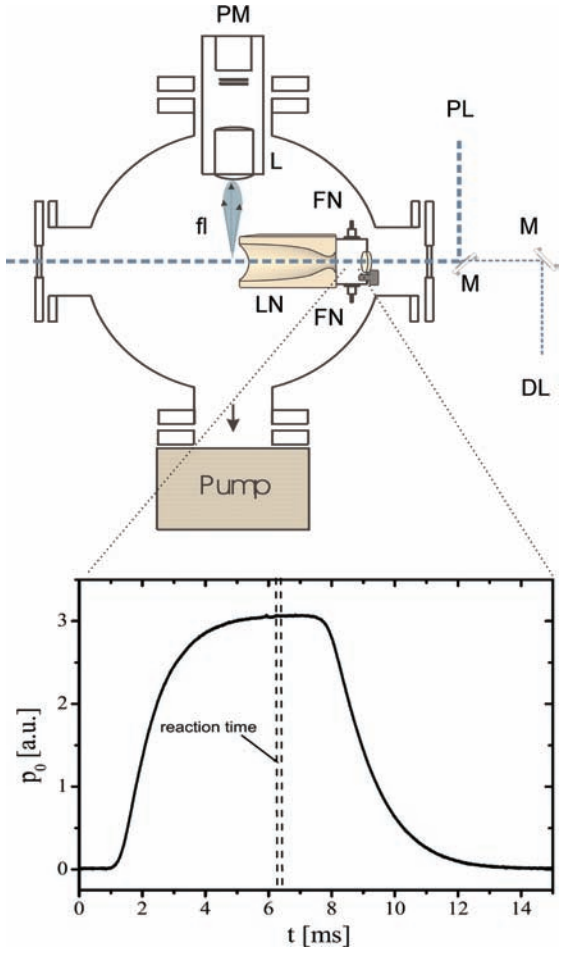

Figure 1. Experimental setup of the pulsed Laval nozzle machine in Göttingen: L, lens; M, mirror; LN, Laval nozzle; FN, feeding nozzles; PM, photomultiplier; PL, photolysis laser; DL, detection laser. The inset (lower panel) displays the time-resolved gas pulse as measured with a pressure impact detector and the measurement and reaction time.

between Mach number and temperature, pressure, and density before (subscript 0) and after the expansion (subscript i) are given as

$$\frac{T_0}{T} = 1 + \frac{\gamma - 1}{2}M^2 \tag{2}$$

$$\frac{p_0}{p} = \left(\frac{T_0}{T}\right)^{\gamma/(\gamma-1)} \tag{3}$$

$$\frac{\rho_0}{\rho} = \left(\frac{T_0}{T}\right)^{1/(\gamma-1)} \tag{4}$$

The nozzles (aluminum with eloxadized surfaces) such as used in the Göttingen experiments are designed according to the method of Moger and Ramsay[23] and manufactured in a workshop with CNC manufacturing technology. They are mounted in a stainless steel block movable 16 cm along the nozzle axis. It contains the stagnation reservoir filled by two pulsed valves, denoted as FN in Figure 1. One of them is a modified car injection valve (BOSCH) supplying carrier gas and the radical precursor (e.g., hydrogen peroxide), and the other one is a General Valve Series 9 valve providing the premixed reactant gas. The duration of the gas pulses is set to 7−10 ms to ensure constant flow conditions for the time-resolved measurements with a maximum delay time of 70 μs. A single pressure pulse is displayed in Figure 1, which shows the plateau of constant flow important for kinetic measurements (thermalization of reactants). Calibrated mass flow controllers (TYLAN) and pressure gauges monitor the gas supply of the injection valves. From the known mass flows in the experiment and photolysis quantum yields the concentration of reactants in the beam could be determined precisely. A KrF excimer laser operating at 248 nm is conveniently used for photolysis of the precursor (PL) and a Nd:YAG laser pumped frequency doubled dye laser for LIF excitation of OH at 282 nm (DL). Quartz windows are mounted at the backside of the stagnation reservoir (Figure 1) and at both ends of the chamber in order to overlap the two laser beams axially in the center of the cold gas flow. The laser-induced fluorescence of OH (308 and 277 nm) monitoring the consumption of OH is imaged from a spatially narrow region of the gas flow. Without reaction (reactant) the fluorescence is stable in time and space to a few percent. The fluorescence light (fl) passes an f:1 optics (L), a bandpass, and interference filter and is detected by a photomultiplier (PMT). The signal is fed into a Boxcar integrator and averaged typically over 250−1000 laser shots. The time resolution (delay step of the two lasers) is adjusted between 1 μs and 100 ns.

The pure amino acid ester tends to oligomerize at ambient temperatures; therefore it was stored at −20 °C. The possible product of an oligomerization, i.e., ethanol and alanine oligomers are relatively unreactive or not particularly volatile. With NMR spectroscopy we could not find any traces of ethanol in the samples. In all experiments fresh samples of alanine ethyl ester were used.

3. Computational Methods

The Gaussian 03 suite of programs is utilized to perform ab initio molecular orbital calculations on L-alanine and L-alanine ethyl ester, radical, prereactive complex, and transition state structures. Geometry optimizations and frequency calculations are carried out by using second-order Møller−Plesset perturbation (MP2) with all electrons unfrozen in the electron correlation. Preliminary optimizations and searches for transition states and prereactive complexes are performed at the MP2 level of theory using the 6-31G(d) basis set. Vibrational frequency calculation at this level of theory is performed to verify whether structures had all positive frequencies for a global minimum or one imaginary frequency for a first-order saddle point, i.e., a transition state. All optimizations are carried out to better than 0.001 Å for bond lengths and 0.1 Å for angles, with self-consistent-field convergence criteria of at least 10^{-7} on the density matrix and a residual rms (root-mean-square) force of less than 10^{-4} au. The proper connectivity between reactants, prereactive complexes, transition states, and products is verified by intrinsic reaction coordinate (IRC) calculations. The minimum energy structures obtained from intrinsic reaction coordinates runs where they used to do full optimization and frequency calculations to identify the pre- and postreactive complexes connected to the transition states. The structures are refined by optimizations at the MP2/6-311G(2d,2p) level of theory. To refine the energy values, single point calculations with higher levels of electron correlation, i.e. coupled cluster theory including singles, doubles, and perturbative corrections for triplets [CCSD(T)] are performed with the 6-311++G(2d,2p) basis set. The degree of spin contamination is monitored because of the possible production of inaccurate total energies. For open shell systems, the $\langle S^2 \rangle$ value did not deviate by more than 3% from the 0.75 value.

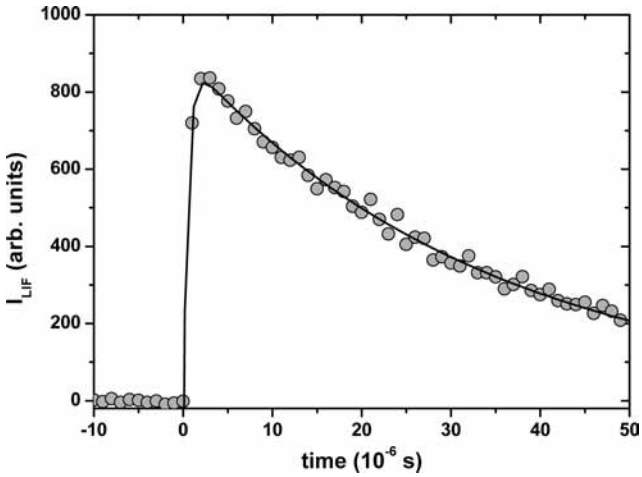

Figure 2. LIF signal of OH radicals in the reaction with alanine ethyl ester in the cold Laval nozzle gas flow as a function of delay time between the photolysis laser and the LIF laser (experimental conditions: $T = 91$ K, $\rho_{OH} = 0.5 \times 10^{11}$ cm^{-3}, $\rho_{AEE} = 3.9 \times 10^{12}$ cm^{-3}, $\rho_{tot} = 0.9 \times 10^{17}$ cm^{-3}). The solid line represents an exponential fit through the data.

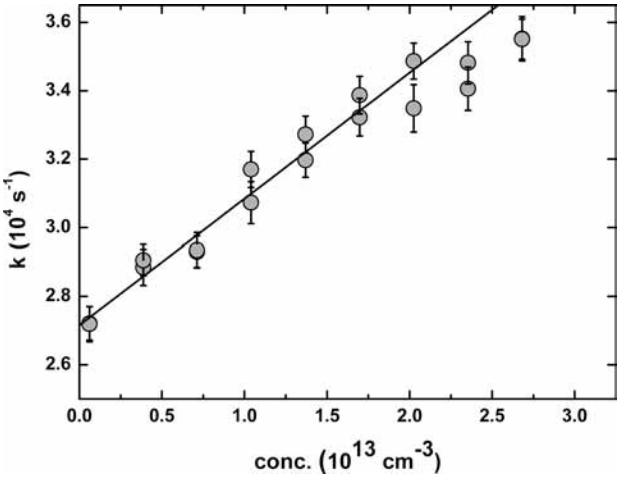

Figure 3. Reaction of OH radicals with alanine ethyl ester in the cold Laval nozzle gas flow. Pseudo-first-order rate constant as a function of reactant (alanine ethyl ester) concentration (buffer gas N_2) for 91 K.

Enthalpies of reaction, prereactive complex energies, and activation energy barriers are corrected with zero-point energies (ZPE), calculated at the UMP2/6-31G(d) level of theory to characterize the energetics of the critical points of the potential energy surface of the reaction of L-alanine and L-alanine ethyl ester with OH radical.

4. Results and Discussion

Since the vapor pressure of amino acid esters is significantly larger than that of amino acids, we have investigated the reaction of OH with L-alanine ethyl ester in our Laval nozzle machine at low temperatures (58 K < T < 300 K). Figure 2 shows experimental data of the reaction of the amino acid ester and the hydroxyl radical in the gas phase. While Figure 2 displays an example for the pseudo-first-order reaction kinetics, Figure 3 displays first-order rate constants as a function of concentration. From the slope of the plot in Figure 3 the second-order rate constant is derived which is plotted in Figure 4 as a function of temperature. All measured second-order rate constants together with the experimental conditions are summarized in Table 1. The reaction in general shows a negative temperature

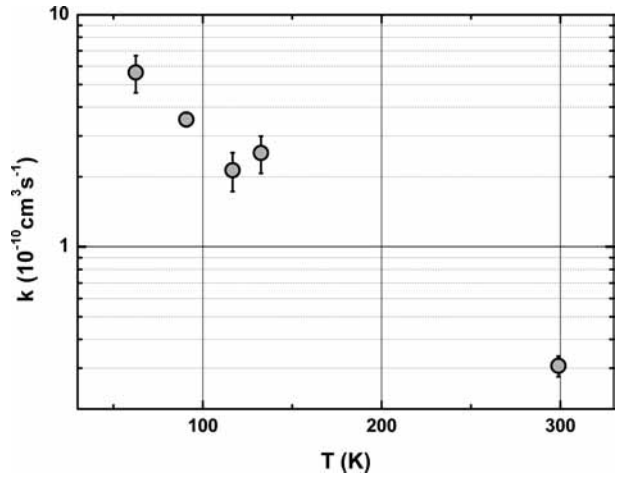

Figure 4. Reaction of OH radicals with alanine ethyl ester in the cold Laval nozzle gas flow. Temperature dependence of the second-order rate constant between 58 and 300 K.

TABLE 1: Rate Constants for the Reaction of OH and L-Alanine Ethyl Ester and Experimental Conditions

T/K	$\rho_{ges}/10^{17}$ cm^{-3}	$k/10^{-10}$ cm^3 s^{-1}	no. of measurements
298	3.4	0.31 ± 0.031	5
133	1.3	2.53 ± 0.46	5
117	0.7	2.13 ± 0.40	7
91	1.1	3.53 ± 0.24	5
60	0.6	5.64 ± 1.0	3

dependence, which has been observed in other complex-forming reactions involving OH-reactions as well.[21,22]

The pronounced negative temperature dependence of the reaction together with the theoretical work of Galano et al.[17] again suggests that prereactive complexes (here hydrogen bound complexes) in combination with a reef-type barrier may be responsible for the experimental data shown in Figure 4.

The optimized geometries of L-alanine and L-alanine ethyl ester are shown in Figure 5. Bond lengths C_α—C_β (1.518 Å for L-alanine and 1.521 Å for L-alanine ethyl ester) and C_α—N (1.455 Å for L-alanine and 1.456 Å for L-alanine ethyl ester) show similarity in structure. Evidence of the C═O characteristic of amino acids is supported by its short bond length (1.219 Å for L-alanine and 1.221 Å for L-alanine ethyl ester). Essential bond lengths found from optimization of L-alanine and L-alanine ethyl ester for the hydrogen on the α carbon (C_α), the β carbon (C_β), and nitrogen all show very little change (the mean deviation is 0.000242 Å). From these optimized geometries, it is evident that the presence of an ethyl group in place of hydrogen on the OH group does not significantly change the geometry of the molecule.

Hydrogen abstraction from the C_α in L-alanine is achieved via a five-membered ring transition state (Figure 6). The ring is stabilized by weak H···N attraction (2.432 Å). The hydrogen being abstracted orients itself closer (1.202 Å) to the C_α than to the radical. The transition state for abstraction from the C_β forms a six-membered ring, stabilized by O−H···N hydrogen bonding. The hydrogen being abstracted is equidistant (1.240 Å) from the L-alanine and the radical. All other essential parameters remain unchanged. The transition state for hydrogen abstraction off the nitrogen demonstrates O−H···O hydrogen bonding to form a seven-membered ring, with the abstracted hydrogen aligning itself more closely to the L-alanine molecule (1.136 Å).

Transition state structure for the abstraction of hydrogen from C_α in the L-alanine ethyl ester has a five-membered ring. The

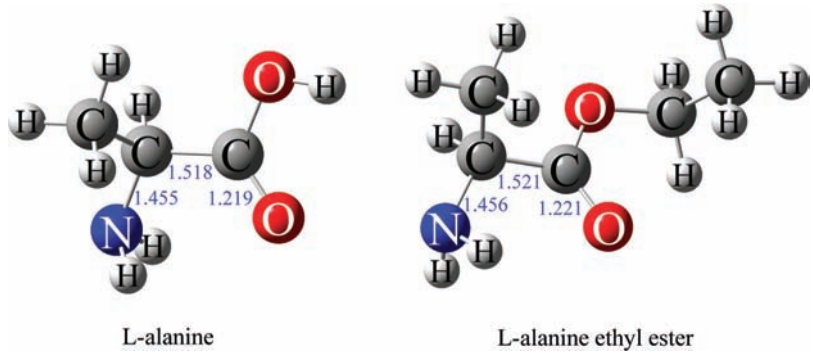

Figure 5. Optimized geometries of L-alanine and L-alanine ethyl ester.

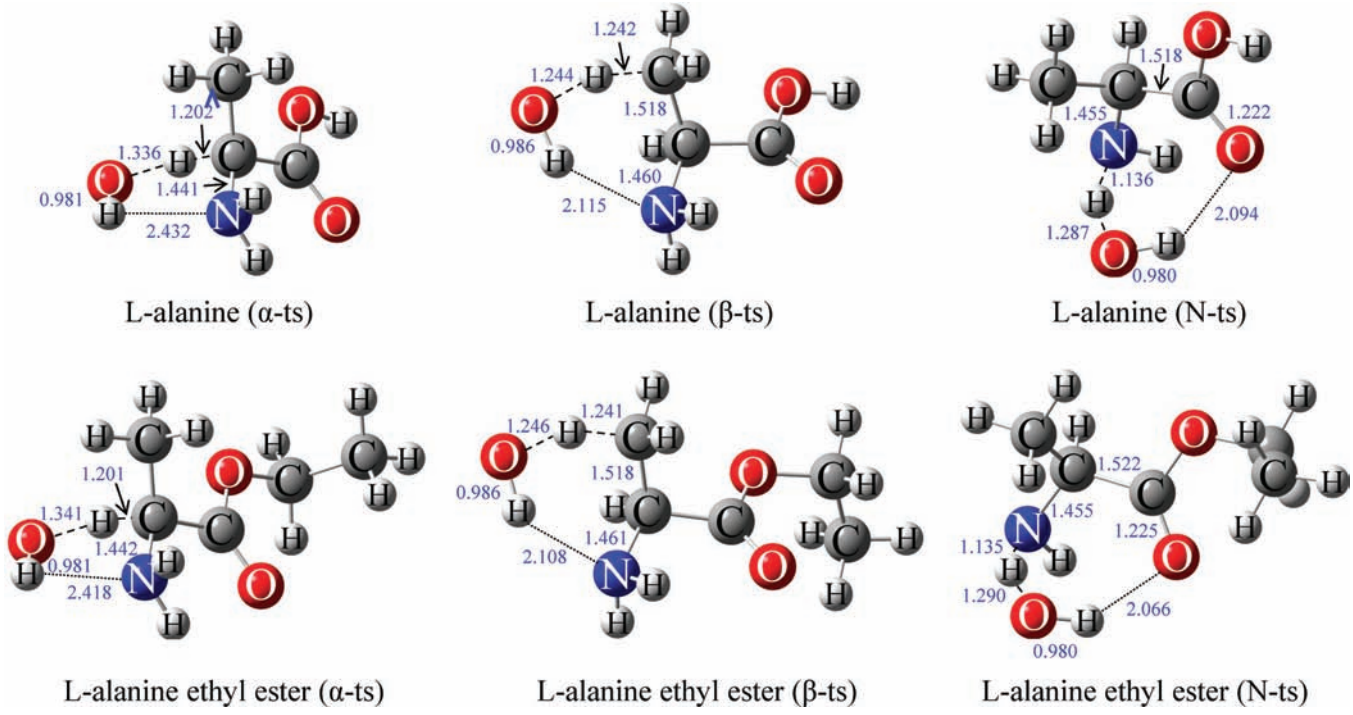

Figure 6. Optimized geometries of transition states of H-abstraction by OH from L-alanine and L-alanine ethyl ester.

TABLE 2: Relative Energetics for L-Alanine + ˙OH and L-Alanine Ethyl Ester + ˙OH

	heat of reaction			prereactive complex			activation energy barriers		
	MP2/ 6-31G(d)	MP2/ 6-311G(2d,2p)	CCSD(T)/ 6-311++G(2d,2p)	MP2/ 6-31G(d)	MP2/ 6-311G(2d,2p)	CCSD(T)/ 6-311++G(2d,2p)	MP2/ 6-31G(d)	MP2/ 6-311G(2d,2p)	CCSD(T)/ 6-311++G(2d,2p)
A-αrad	−32.1	−37.9	−42.7	−12.5	−12.3	−18.8	4.6	1.1	−6.8
A-βrad	−10.6	−16.4	−21.2	−16.7	−15.6	−19.9	6.3	2.2	−4.0
A-Nrad	−13.3	−16.3	−22.8	−15.0	−14.0	−18.2	4.0	0.7	−7.0
AEE-αrad	−31.6	−37.4	−35.7	−13.2	−13.0	−11.6	4.3	0.8	−1.0
AEE-βrad	−10.6	−16.4	−15.0	−16.8	−16.6	−13.9	6.1	2.0	1.9
AEE-Nrad	−13.5	−16.5	−16.9	−15.3	−14.4	−12.4	3.5	0.3	−1.3

radical aligns itself such that a slight attraction occurs between the radical hydrogen and the amide, while the abstracted hydrogen remains closer (1.201 Å) to the L-alanine ethyl ester than to the radical. The hydrogen abstracted from C_β is equidistant between the radical and the L-alanine ethyl ester molecule in the transition state structure. Interestingly, O−H···N hydrogen bonding (2.108 Å) stabilizes the six-membered ring, which otherwise has essential parameters unchanged from the optimized L-alanine ethyl ester molecule. The transition state structure for hydrogen abstraction off the nitrogen contains strong hydrogen bonding in its seven-membered ring. One general trend among transition states of both alanine and its ethyl ester is the ring structure formed as the radical attacks—the C_β and N is stabilized by hydrogen bonding.

The transition state structures for H-abstraction off the α carbon, β carbon, and nitrogen of L-alanine and L-alanine ethyl ester appear similar. For example, the C_α−H bond being abstracted in the transition state in L-alanine is 1.202 Å while in L-alanine ethyl ester it is 1.201 Å. The OH bond being formed in the transition state for the α carbon abstraction is 1.336 Å for L-alanine and 1.341 Å for L-alanine ethyl ester. Similar comparisons for the essential transition state features for the β carbon and nitrogen hydrogen abstractions show a mean deviation of 0.000325 Å. These results suggest that the substitution of the ethyl group does not significantly alter the transition states for hydrogen abstractions for L-alanine and L-alanine ethyl ester. This has some very important ramifications for experimental studies of biomolecules, in particular experi-

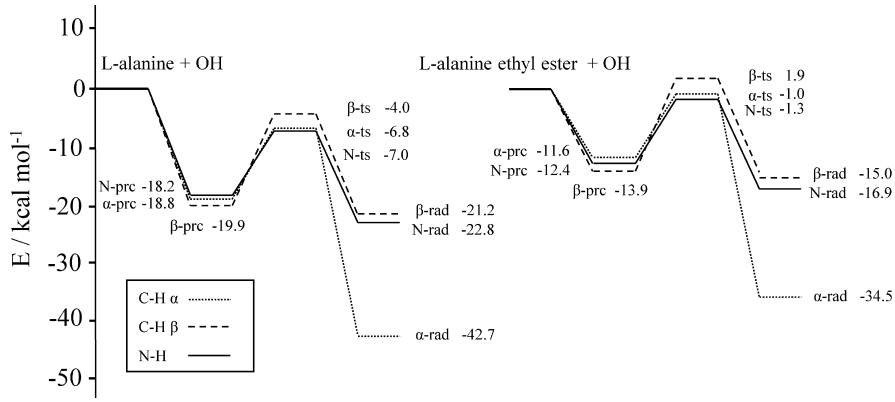

Figure 7. Potential energy surface of L-alanine + OH and L-alanine ethyl ester + OH.

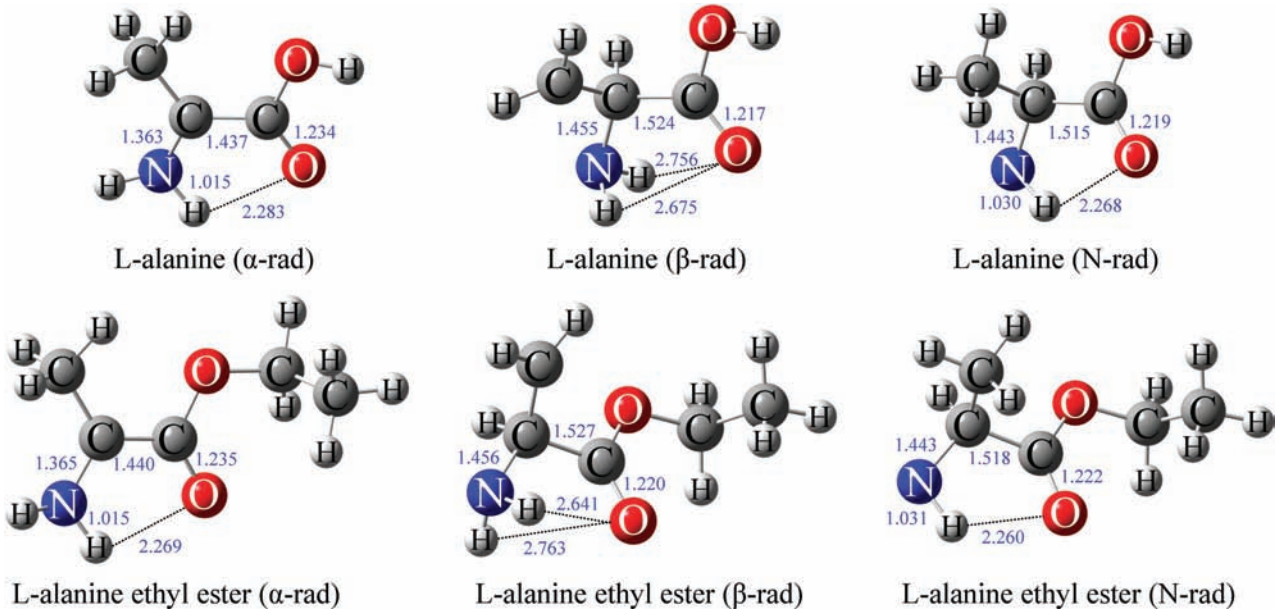

Figure 8. Optimized geometries of radicals formed by H-abstraction from L-alanine and L-alanine ethyl ester.

mental studies of small amino acids, which are difficult to isolate in the gas phase for quantitative studies of the reactivity. This study suggests that studies of the amino acid esters, because they have significantly larger vapor pressures than the amino acids, are also good models for understanding the kinetics of the amino acids in the gas phase.

Our results suggest that structural features of L-alanine are applicable to the L-alanine ethyl ester. If the calculations by Galano et al. are also applicable to the amino acid ester, the OH attack and H-abstraction at the α-carbon atom is slightly preferred over the attack at the β-methyl carbon atom. In any case the height of the barriers and not the energetics of the intermediate products determines the (relative) rate constants of the reaction. The temperature dependence of the reaction rate constant suggests a barrier height that is lower than the energy of the reactants. As far as the relative rates and reaction sites are concerned, it should be noted that the energy of the transition state TSβ (in the calculations of Galano et al.) is somewhat higher but still close to the energy of TSα, although the energy of the final radicals is very much different, making a unique and exclusive attack at one site less likely.

This work shows that MP2/6-31G(d) energetics alone are insufficient to reliably estimate the barrier for OH reaction with L-alanine and L-alanine ethyl ester. The data in Table 2 indicate both a basis set and electron correlation effect on the barriers for both L-alanine and L-alanine ethyl ester. The studies of L-alanine by Galano et al.[17] show that the abstraction of the α-carbon is preferred over the β-site. Galano et al. did not examine abstraction at the nitrogen site. At the MP2/6-31G(d) level of theory, our finding that α-site abstraction is preferred over the β-site abstraction is consistent with the conclusion of Galano et al. However, these barriers are 4 kcal/mol over the reactants level. Those findings are inconsistent with the temperature dependence of the reactions rate constant experimental results, which suggest that the barrier height is lower than the energy of the reactants. At the MP2/6-311G(2d,2p) level of theory, the barrier reduces but is still above the reactants. At the CCSD(T)/6-311++G(2d,2p) level of theory, we find that for L-alanine all the barriers are below the reactants level.

For L-alanine ethyl ester, the barriers at the MP2/6-31G(d) level of theory are similarly 3.5 kcal/mol above the reactants level. With the MP2/6-311(2d,2p) level of theory, barrier heights decrease to slightly over 0 kcal/mol, and barrier heights for hydrogen abstraction off the N-site and the α-carbon site move below the reactants level at the CCSD(T)/6-311G++(2d,2p) level of theory. The N-site is kinetically favorable but competitive with the α-carbon site. The β-site, however, is 1.9 kcal/mol above the reactant level, suggesting that the β-site abstract is the least preferred site for hydrogen abstraction off of L-alanine ethyl ester.

The preferred site of hydrogen abstraction in both L-alanine and L-alanine ethyl ester is the N-site (barrier energy of −7.0 kcal/mol for L-alanine and −1.3 kcal/mol for L-alanine ethyl ester) with competition from the α-carbon site (−6.8 and −1.0 kcal/mol). These findings are consistent with those conclusions from studies that find the N-site or α-carbon site as the site of attack. While the barrier energies for L-alanine are lower than those for L-alanine ethyl ester, the two are proportionately the same. Thus the relative energetics of L-alanine ethyl ester demonstrates that L-alanine ethyl ester can serve as a good model for L-alanine.

The experiments also show a negative temperature dependence, which suggests the formation of complexes involving OH and L-alanine ethyl ester. Prereactive complexes are found for the α-carbon site and N-centered radical site. These prereactive complexes are quite stable, exhibiting a well depth of −18.8 kcal/mol for the α-carbon site and −14.0 kcal/mol for the N-centered radical site for L-alanine, and the L-alanine ethyl ester shows similar binding energies for the prereactive complexes. These findings are consistent with the experiments that demonstrate the presence of prereactive complexes.

Interestingly, Galano et al. also calculated rate constants for the reaction of amino acids with OH in the gas phase, employing conventional transition state theory,[17] which are at least 1 order of magnitude lower (at room temperature) than the rate constants measured for OH + alanine ethyl ester in our present Laval nozzle experiments. Since the barriers of the alanine ethyl ester are found to be higher than those of the amino acid, one may expect that the reaction of the latter with OH may be indeed faster.

In summary, we have shown that reactions of the OH radical with amino acid derivatives (here employed due to the larger vapor pressure) can be measured in the gas phase. Calculations for the amino acid and the amino acid ester suggest that the esters are indeed good kinetic model systems for amino acids and that the ester group (at least for alanine ethyl ester) does not influence the H-atom abstraction dynamics significantly. Contrary to the accepted view that OH radical attack prefers the C_α-site, the present work finds that for both L-alanine and L-alanine ethyl ester the N-site is competitive with the C_α-site. This is important new insight into understanding oxidative damage of (L-alanine) amino acids in the presence of free OH radicals.

Acknowledgment. B.A., B.H., and M.L. gratefully acknowledge support from the Deutsche Forschungsgemeinschaft DFG (Graduiertenkolleg 782) and interesting discussions with Professor J. Troe and Professor R. B. Gerber.

References and Notes

(1) Finkel, T.; Holbrook, N. J. *Nature* **2000**, *408*, 239–248.
(2) Garrison, W. M. *Chem. Rev.* **1987**, *87*, 381–398.
(3) Rauk, A.; Yu, D.; Armstrong, D. A. *J. Am. Chem. Soc.* **1997**, *119*, 208–217.
(4) Potashkin, J.; Meredith, G. E. *Antioxid. Redox Signaling* **2006**, *8* (1, 2), 144–151.
(5) Stefanic, I.; Bonifacic, M.; Asmus, K. D.; Armstrong, D. A. *J. Phys. Chem. A* **2001**, *105*, 8681–8690.
(6) Gancheva, V.; Sagstuen, E.; Yordanov, N. D. *Radiat. Phys. Chem.* **2006**, *75*, 329–335.
(7) Goshe, M. B.; Chen, Y. H.; Anderson, V. E. *Biochemistry* **2000**, *39*, 1761–1770.
(8) Joshi, A.; Rustgi, S.; Moss, H.; Riesz, P. *Int. J. Radiat. Biol.* **1978**, *33* (3), 205–229.
(9) Rustgi, S.; Joshi, A.; Moss, H. R. P. *Int. J. Radiat. Biol.* **1977**, *31* (5), 415–440.
(10) Steffen, L. K.; Glass, R. S.; Sabahi, M.; Wilson, G. S.; Schöneich, C. M. S.; Asmus, K. D. *J. Am. Chem. Soc.* **1991**, *113*, 2141–2145.
(11) Begusova, M.; Giliberto, S.; Gras, J.; Sy, D.; Charlier, M.; Spotheim-Mauriozot, M. *Int. J. Radiat. Biol.* **2003**, *79* (6), 385–391.
(12) Cruz-Torres, A.; Galano, A.; Alvarez-Idaboy, J. R. *Phys. Chem. Chem. Phys.* **2006**, *8* (2), 285–292.
(13) Galano, A.; Alvarez-Idaboy, J. R.; Agacino, E.; Ruiz-Santoyo, M. E. *Rev. Soc. Quim. Mex.* **2004**, *48* (2), 139–145.
(14) Galano, A.; Alvarez-Idaboy, J. R.; Agacino-Valdes, E. R.; -S, M. E. *THEOCHEM* **2004**, *676* (1−3), 97–103.
(15) Galano, A.; Alvarez-Idaboy, J. R.; Bravo-Perez, G.; Ruiz-Santoyo, M. E. *THEOCHEM* **2002**, *617*, 77–86.
(16) Galano, A.; Alvarez-Idaboy, J. R.; Cruz-Torres, A.; Ruiz-Santoyo, M. E. *THEOCHEM* **2003**, *629*, 165–174.
(17) Galano, A.; Alvarez-Idaboy, J. R.; Montero, L. A.; Vivier-Bunge, A. *J. Comput. Chem.* **2001**, *22*, 1138–1153.
(18) Galano, A.; Alvarez-Idaboy, J. R.; Torres-Cruz, A.; Ruiz-Santoyo, M. E. *Int. J. Chem. Kinet.* **2003**, *35* (5), 212–221.
(19) Nukuna, B. N.; Goshe, M. B.; Anderson, V. E. *J. Am. Chem. Soc.* **2001**, *123*, 1208–1214.
(20) Voehringer-Martinez, E.; Hansmann, B.; Hernandez, H.; Francisco, J. S.; Troe, J.; Abel, B. *Science* **2007**, *315*, 497.
(21) Spangenberg, T.; Koehler, S.; Hansmann, B.; Wachsmuth, U.; Abel, B.; Smith, M. A. *J. Phys. Chem.* **2004**, 7527.
(22) Hansmann, B.; Abel, B. *ChemPhysChem* **2007**, *8*, 343–356.
(23) Moger, W. C.; Ramsay, D. B. *Report No. AEDC-TDR-64-110*, Arnold Engineering Development Center: Tullahoma, TN 1964.

JP9015596